Application of Controlled-Drift Detectors in Diffraction Enhanced Imaging of Tissues

A. Castoldi, *Member, IEEE*, C. Guazzoni, *Member, IEEE*, A. Galimberti, R. Hartmann, S. Pani, G. Royle, and L. Strüder

***Abstract*—Diffraction Enhanced Breast Imaging could potentially give a significant increase in sensitivity and specificity compared to conventional transmission x-ray mammography. A device that may be promising for this application area is the Controlled-Drift Detector. The Controlled Drift Detectors feature a small pixel size, similar to Charge Coupled Devices, but are superior to Charge Couple Devices in certain key areas: (a) they can operate in photon counting mode measuring the energy with spectroscopic resolution, (b) very high frame rates are possible (up to 100 kHz) and (c) they can potentially be constructed to large area linear devices. The results of the first performance evaluation of the Controlled Drift Detector in its application to Diffraction Enhanced Breast Imaging are presented and discussed.**

***Index Terms*—Controlled-Drift Detector, DEBI, X-ray imaging.**

I. Introduction

The use of X-rays in medical applications is usually limited to transmission imaging and scattered photons are considered a drawback that decreases the image contrast. However, scattered photons, differently from the primary transmitted beam, interact with the tissue under analysis and can therefore yield specific information on its molecular structure. This is of particular interest in the analysis of breast tissue. Conventional mammography is currently considered the most effective breast screening tool. However, it has drawbacks and alternative techniques are being sought for improving tissue discrimination.

Mammograms vary in appearance by the amount and distribution of fat and fibro-glandular tissue. While a tumour can usually be easily detected in a predominantly fatty breast due to the large difference in the attenuation coefficients of the two tissue types, the detection of a tumour in a denser breast becomes difficult due to the small difference in the attenuation coefficients of carcinoma and fibroglandular tissue [1].

For this reason, alternative techniques are being sought for obtaining higher diagnostic accuracy, particularly for women with dense breasts.. Among these, Diffraction Enhanced Breast Imaging (DEBI) may be a promising alternative [2-5]. The main limitation of DEBI is the low yield of scattered photons for a given angular aperture. For this reason, the choice of a suitable detector is of crucial importance.

In this paper we present the first results of an experimental evaluation of the Controlled-Drift Detector (CDD), a novel X-ray silicon imager, in its application to DEBI. Synchrotron radiation beams were used for testing the performance of the detector under several defined conditions, but DEBI is likely to be implemented also on conventional sources using a CDD. Section II reviews the advantages and constraints of DEBI and Section III highlights the basic features of the Controlled-Drift Detector and the advantages of its use in this analytical technique. Section IV is devoted to the assessment of the use of this novel detector type in Diffraction Enhanced Imaging through experimental measurements on phantoms. Section V presents the results of the application of Controlled-Drift Detectors to diffraction-enhanced imaging of biological tissues. Section VI ends with the indication of future developments.

II. Advantages and Constraints of DEBI

Coherent scattering is described classically as the interaction between the electric field associated with the x-ray beam and the electric field associated with the electron charge distribution in the material [6]. The electrons are set oscillating and subsequently emit radiation of the same wavelength as the incident beam. In biological materials, coherent scatter becomes important at photon energies below 50 keV and, because of its sharply forward peaked nature; it is the dominant scattering process at small angles (up to 10°).

Manuscript received January 23, 2007. This work was supported in part by INFN, Sezione di Milano and by a Marie-Curie Intra-European Fellowship within the 6th European Community Framework Programme under Grant No. MEIF-CT-2004-007206.

Andrea Castoldi and Antonio Galimberti are with Dipartimento di Ingegneria Nucleare, Politecnico di Milano and INFN, Sezione di Milano, 20133 Milano, Italy (telephone +39 02 23996321, e-mail andrea.castoldi@polimi.it).

Chiara Guazzoni is with Dipartimento di Elettronica e Informazione, Politecnico di Milano and INFN, Sezione di Milano, 20133 Milano, Italy. (telephone: +39 02 23996147, e-mail: chiara.guazzoni@mi.infn.it).

Robert Hartmann is with PNSensor GmbH, and with [f]MPI Halbleiterlabor, Otto-Hahn-Ring 6, 81739 München, Germany.

Silvia Pani and Gary Royle are with the Department of Medical Physics and Bioengineering, University College London, WC1E 6BT London, UK (e-mail: spani@medphys.ucl.ac.uk, groyle@medphys.ucl.ac.uk).

Lothar Strüder is with Max Planck Institut Halbleiterlabor, Otto-Hahn-Ring 6, München D-81739, Germany and with Max Planck Institut für Extraterrestriche Physik. He is also with Universität Siegen, FB Physik.

The interference of scattered photons gives rise to diffraction patterns. These patterns provide a unique signature characteristic of the material that has been irradiated. In the case of a structure with a short-range order, such as biological tissue, the distribution of the scattered intensity is characterized by one or more smooth peaks at well-defined values of the momentum transfer $\chi = 1/\lambda \sin(\theta/2)$ where λ is the beam wavelength and θ is the scattering angle.

In the case of breast tissue, the maximum differences in the scattered signal from normal tissue and carcinoma are detected when the momentum transfer is $\chi = 1.1$ nm^{-1}, and $\chi = 1.7$ nm^{-1}, as shown in Fig. 1 [7]. At $\chi = 1.1$ nm^{-1}, the signal from normal tissue is about twice the signal from carcinoma, while at $\chi = 1.7$ nm^{-1} the diffracted intensity from carcinoma is about 1.5 times higher than that from healthy tissue. At $\chi = 1.3$ nm^{-1}, the signal from normal tissue is nearly equal to the signal from carcinoma. In the following sub-sections we illustrate the advantages and drawbacks of traditional DEBI analysis to motivate the advantages of the application of a novel detector to DEBI.

A. *Energy Dispersive DEBI*

Fig. 2a shows a schematic representation of the setup used in Energy Dispersive DEBI. A polychromatic X-ray pencil beam illuminates the sample and the photons scattered at a given angle (selected with a conical collimator) are detected with an energy dispersive detector (e.g. HPGe detector). The main advantages of this technique are the use of a conventional source as the primary beam and the possibility of investigating simultaneously several momentum transfer values. Unfortunately the technique has no position discrimination capability; therefore it can be used in the study of homogenous media to determine the material linear differential scatter coefficient but does not provide imaging information unless the sample is scanned in front of the beam, which implies longer acquisition times.

B. *Synchrotron radiation DEBI*

Fig. 2b shows a schematic representation of the setup used in synchrotron radiation DEBI. The primary radiation is a monochromatic laminar beam from a synchrotron source. A position-sensitive detector, coupled to a multi-hole collimator, is used. Different values of the momentum transfer are achieved by changing either the beam energy or the scatter angle θ. This technique can be used to obtain diffraction images of the sample under analysis. The implementation of this technique with conventional x-ray sources imposes more strict requirements on the detector side in terms of energy and position resolution. The low noise CCD currently used for this setup (x-ray sensitive L3Vision CCD camera [8]) has very good position resolution, but features no energy discrimination capabilities.

III. Basic Features and Performance of Controlled-Drift Detectors

In this Section we present the working principle and the main features of a recently proposed X-ray detector [9] featuring 2-D position resolution and energy resolution that can be employed to improve traditional DEBI analysis but may also fulfill the requirements of DEBI setup with conventional x-ray sources.

The Controlled-Drift Detector [10-12], schematically shown in Fig.3, is built on a fully depleted high-resistivity silicon wafer (300-450 μm wafer thickness) that assures a good quantum efficiency in the 1-30 keV range. Its working principle is based on the generation of equally spaced potential wells along the drift direction during the integration phase and on the transport of the charge packets stored in each pixel by means of an electrostatic field during the readout phase (integrate-readout mode). The removable confinement along the drift direction is provided by an externally controlled perturbation applied to the linear drift potential. The permanent confinement in the direction transversal to the drift is obtained with a suitably tailored pattern of deep p- and n-implants. The detector operates in single-photon counting mode. That is, for each detected X-ray photon, the incident position along the drift direction is given by the measurement of the electron drift time while the X-ray energy is obtained from the measurement of the deposited charge. The second spatial coordinate is obtained from the granularity of the readout anodes. The anode capacitance can be made very small (of the order of 100 fF) and independent of the active area of the detector which, together with the on-chip JFET for signal amplification, allows one to reach excellent energy resolution as in a conventional Silicon Drift Detector [13].

The achievable performance of this kind of detector has been assessed in terms of energy resolution, position resolution and maximum event rate [9-12, 14-16] with extended tests in the lab and with synchrotron light of different Controlled-Drift Detector prototypes. Drift velocities in the range 0.3-0.5 cm/μs have been measured and lead to readout times of the order of 2-3 μs for a 1 cm-long detector. This readout mechanism is inherently faster than the one of a charge-coupled device as it allows integration times of only few tens of μs. This feature allows detector operation at room temperature while having an energy resolution close to the one obtainable with state-of-the-art fully-depleted pn-charge-coupled devices [17] typically operating at cryogenic temperatures and lower frame frequency (i.e. the reference device for high resolution x-ray imaging and spectroscopy). To evaluate the achievable detector performance we irradiated a 6x6 mm^2 CDD with 180μm x 180μm pixels with a ^{241}Am source. The measurement has been performed at RT with a detector frame frequency of 67 kHz and an integration-readout ratio of 9. The RT energy res. was 515 eV FWHM at the 13.9 keV line of which the contribution of the RT detector leakage current is dominant over the other noise sources. For more demanding spectroscopic applications the best energy resolution can be reached by moderately (Peltier) cooling the detector.

The possibility of energy discrimination allows wider and more powerful experimental implementations of DEBI. DEBI

setup with conventional X-ray sources becomes possible as the detector energy resolution allows selection of a narrow momentum transfer window (i.e., the order of 1% at 18 keV at room temperature and better with moderate cooling). An X-ray source with a broad energy spectrum together with a Controlled Drift Detector would therefore provide images of the sample at multiple specified values of the momentum transfer at the same time or the full diffraction intensity distribution for each voxel.

IV. Assessment of using Controlled-Drift Detectors in Diffraction- Enhanced Imaging

In order to investigate the use of CDD in DEBI and probe its potential we evaluated its performance in synchrotron DEBI. Fig. 4 gives a schematic representation of the experimental setup that we built at the SYRMEP beamline of the ELETTRA synchrotron source in Trieste (Italy). Data acquisition was performed during a single run in April 2005. A tungsten slit system, located at the entrance of the experimental hutch, was used to obtain a laminar beam (500 μm thick for diffraction images and about 5 mm thick for transmission images). The CDD was mounted on a goniometric cradle used to tilt the system at 9 degrees for the acquisition of diffraction images. A multi-hole brass collimator (500 μm hole - 500 μm spacing) was placed in front of the CDD to acquire the diffraction images. A rotary stage was used to align the detector+collimator system with respect to the beam. Both diffraction and transmission images were acquired with the CDD. Transmission images were acquired with the collimator removed and with the detector parallel to the primary beam. Diffraction images were acquired with the CDD by vertically scanning the sample in front of the beam. For each vertical position, two images, with a 500 μm horizontal displacement of the sample, were acquired, in order to cover the whole sample area. Two beam energies were used to define the required momentum transfer (18 keV for χ=1.1 nm^{-1} and 26 keV for χ=1.7 nm^{-1}).

For each detector pixel we selected the counts within an energy window of 5 keV centered at the photo-peak energy. All pixel counts corresponding to the same collimator hole were summed; hence, each line of a diffraction image consisted of 12 pixels 500 μm × 500 μm in size. All images were corrected for beam-intensity and detector-response non-uniformity by means of a flat-field image; for diffraction images the flat-field image was obtained with a uniform scatterer in front of the detector.

The Controlled-Drift Detector prototype used for the present study had a 180 μm × 180 μm pixel size and a total area of 3.96 mm × 6.12 mm (22×34 pixels). The detector thickness was 300 μm, allowing a photon absorption efficiency of about 30% at 18 keV and 14% at 26 keV, respectively. The drift field was set to 400 V/cm, allowing a frame rate of 50 kHz. The measured energy resolution was about 2.15 keV FWHM at 18 keV at room temperature due to excessive leakage current of the prototype used. Fig. 5 shows the measured spectrum with the detector set either for transmission images acquisition (black line) or for diffraction images acquisition (gray line). The energy was set to 18 keV. The monochromator (Si(111)) does not transmit only the desired fundamental energy, but also higher-order harmonics. Allowed harmonics for Si(111) include (333) and (444). The corresponding peaks in the spectrum are clearly visble. The peak at twice the primary energy is due to pulse pile-up in the detector. No correction for beam intensity is carried out for the two spectra; this is the reason for a higher intensity of the "diffraction" spectrum at 18 keV (photo-peak energy) with respect to the transmission one.

Preliminary test measurements were performed on a perspex phantom with both empty holes and holes filled with water. The first test was made with a perspex phantom 0.5-cm-thick with holes 4, 2 and 1 mm in diameter. Fig. 6a and Fig. 6b show the transmission and the diffraction image acquired at 18 keV. The darker areas (corresponding to a higher exposure) in the transmission image are the holes, which appear brighter (thus representing a lower exposure) in the diffraction image due to the lower scattered intensity from air with respect to perspex. We then performed a second test by filling the holes with water. This measurement is more demanding, as the linear attenuation coefficient of perspex is quite close to that of water at 18 keV (0.82 and 1.00 cm^{-1} respectively) [18]. Only the 4 mm and the 2 mm holes were filled with water because we were not able to fill the 1 mm hole. Fig. 6c and Fig. 6d show the transmission and diffraction images respectively. The darker area (corresponding to a higher exposure) in the bigger hole in the transmission image is due to an air bubble, which appears brighter (thus representing a lower exposure) in the diffraction image due to the lower scattered intensity from air with respect to water. The measured detail-to-background contrast (larger detail in figures 7a, 7b) in the transmission image is 0.13±0.01 and is increased to 0.36±0.01 in the diffraction image.

V. Application of Controlled-Drift Detectors to Diffraction-Enhanced Imaging of Tissues

In order to better assess the performance of the Controlled-Drift Detector in DEBI measurements we analyzed two pork meat samples. The meat sample shown in Fig. 7a was about 5 mm thick and was selected for having two distinct regions of muscle (the bright area in the transmission image) and of fat (the dark area in the transmission image), which feature scattering properties very close to those of tumor and of normal breast tissue respectively [19]. Fig. 7b shows the transmission image of this sample at 18 keV and Fig. 7c shows the diffraction image. Fig. 7d and Fig. 7e show the transmission and diffraction images, respectively, at 26 keV. The diffraction images were slightly misaligned with respect to the transmission ones. The contrast in the two diffraction images is reversed as expected, because the diffraction signal from fat is higher than that from muscle at χ=1.1 nm^{-1}, while the opposite occurs at 1.7 nm^{-1} [2], thereby demonstrating the

sensitivity to tissue type by appropriate choice of momentum transfer.

The second meat sample, shown in Fig. 8a, was a more challenging test structure since it presented a smaller and more complex fat structure nested in the muscle tissue with details less than 1 mm in size. Fig. 8b shows the transmission image of this sample at 18 keV and Fig. 8c shows the corresponding diffraction image. Fig. 8d and Fig. 8e show the transmission and diffraction images, respectively, at 26 keV. Also in this case the diffraction images were slightly misaligned with respect to the transmission ones. We obtained the same behavior as for the previous sample, fat regions being clearly distinguished from muscle ones in the diffraction images. The measured detail-to-background contrast in the transmission image and in the diffraction image for both samples are reported in Table I together with the achieved contrast improvement. The obtained results are fully comparable with the ones reported in [2].

VI. Future developments with conventional X-ray sources and large area detectors

The results previously described encourage us to pursue the application of Controlled-Drift Detectors to DEBI with conventional X-ray sources emitting a broad energy spectrum. The energy resolution achievable with a CDD would provide a momentum transfer resolution of the order of $\Delta\chi/\chi\sim1/100$ in the energy range of interest, the main contribution to the overall momentum transfer resolution being given by the collimator aperture. When the sample is illuminated with a conventional X-ray beam, each pixel records an energy spectrum that is equivalent to the diffracted intensity distribution as a function of the momentum transfer, weighted by the intensity distribution of the incoming spectrum. This allows the simultaneous investigation of several momentum transfer values. The possibility of performing multi-momentum transfer imaging would allow one not only to discriminate between neoplastic and healthy tissue, but also to discriminate between different types of tumor, characterized by different diffraction patterns [7]. As reported in [2]-[5], the DEBI technique is not intended to replace transmission mammography, but to combine diffraction and transmission imaging to enhance image contrast and provide further tissue discrimination. Such a system could also be useful for non-medical applications like material analysis and explosive detection [21]. A novel 3×1 cm^2 Controlled-Drift Detector has been designed and first detector prototypes were recently produced at the Halbleiterlabor of the Max Planck Institut in cooperation with PNSensor GmbH. The detector features 240 drifting columns with 120 μm pitch and a maximum drift length of about 1 cm. The detector thickness has been increased to 450 μm to improve the quantum efficiency (about 45% at 18keV and 18% at 26keV). We plan to test this detector in DEBI measurements with a conventional X-ray source similar to the one used for conventional mammography in the near future.

Acknowledgment

We acknowledge the staff of the Max Planck Institut Halbleiterlabor in Munich together with H. Soltau, P. Holl, and the staff of PNSensor GmbH in Munich for detector production. We want to acknowledge S. Masci for careful and professional detector bonding. We also thank D. Arceri for the help in the development of the DAQ system and A. Vescovi for the help in the experimental measurements. We are indebted to the staff of the SYRMEP beamline at ELETTRA for their kind hospitality.

References

[1] P.C. Johns and M.J. Yaffe, “X-ray characterization of normal and neoplastic breast tissues”, *Phys Med Biol*., 1987, 32, 675-695

[2] G.J.Royle, E.J.Harris, R.D.Speller, J.A.Griffiths and A.M.Hanby, “Diffraction enhanced breast imaging: preliminary results from the Elettra synchrotron source”, 2002 IEEE Nuclear Science Symposium & Medical Imaging Conference Conference Records, Norfolk, Virginia, USA, 2002.

[3] J. A Griffiths, R. D. Speller, G. J. Royle, J. A. Horrocks, A. Olivo, S. Pani, R. Longo, D. Dreossi, D. P. Clifford and A. M. Hanby, “X-Ray Diffraction CT of Excised Breast Tissue Sections: First Results from Elettra”, 2003 IEEE Nuclear Science Symposium and Medical Imaging Conference Conference Records, Portland Oregon, USA, 2003.

[4] J. A. Griffiths, G. J. Royle, R. D. Speller, J. A. Horrocks, A. Olivo, S. Pani, R. Longo, D. Dreossi, D. P. Clifford and A. M. Hanby, “Diffraction Enhanced Breast Imaging: Assessment Of Realistic System Requirements To Improve The Diagnostic Capabilities Of Mammography”, 2003 IEEE Nuclear Science Symposium and Medical Imaging Conference Conference Records, Portland Oregon, USA, 2003.

[5] J. A. Griffiths, G. J. Royle, J. A. Horrocks, A. M. Hanby, R. D. Speller, “Correlation of Diffraction MicroCT Images of Breast Tissue with Pathological Analysis”, 2006 IEEE Nuclear Science Symposium and Medical Imaging Conference Conference Records, San Diego, California, USA, 2006.

[6] S.C. Roy, K. Lynn, R. H. Pratt, “Elastic scattering of photons”, *Radiat. Phys. Chem.*, vol. 56, 1999, pp. 3-26.

[7] G Kidane et al. "X-ray scatter signatures for normal and neoplastic breast tissues", *Phys Med Biol* 1999: 44; 1791-1802.

[8] P. Jerram, P. Pool, R. Bell, D. Burt, S. Bowring, S. Spencer, M. Hazelwood, I. Moody, N. Catlett, P. Heyes, “The LLLCCD: Low light imaging without the need for an intensifier,” SPIE Photonics West Conference, San Jose, USA, 2001.

[9] A. Castoldi, G. Cattaneo, A. Galimberti, C. Guazzoni, P. Rehak, L. Strüder, "Room-temperature 2-D X-ray imaging with the Controlled-Drift Detector", *IEEE Trans. Nucl. Sci*., Vol. 49, no.3, June 2002, 989-994.

[10] A. Castoldi, A. Galimberti, C. Guazzoni, P. Rehak, L. Strüder, “X-ray imaging and spectroscopy with Controlled-Drift Detectors: experimental results and perspectives”, *Nucl. Instrum. Meth*. A512 (1-2), October 2003, pp. 250-256.

[11] A. Castoldi, A. Galimberti, C. Guazzoni, P. Rehak, L. Strüder, "Towards large area X- and Gamma-ray imagers based on Controlled-Drift Detectors", *Nucl. Instrum. Meth*. A518 (1-2), 1 February 2004, pp. 426-428.

[12] A. Castoldi, A. Galimberti, C. Guazzoni, L. Strüder, "Time-resolved X-ray spectroscopic imaging with novel silicon drift detectors", *IEEE Trans. Nucl. Sci*., Vol. 53, no. 1, Feb. 2006, pp. 373-377

[13] P. Lechner, A. Pahlke, H. Soltau, “Novel high-resolution silicon drift detectors”, *X-ray Spectrometry*, Vol. 33, July/August 2004, pp. 256-261.

[14] A. Castoldi, C. Guazzoni, P. Rehak, L. Strüder, "Spectroscopic-grade X-ray imaging up to 100 kHz frame rate with Controlled-Drift Detectors" *IEEE Trans. Nucl. Sci.*, Vol. 48, No. 4, pp. 982-986, August 2001.

[15] A.Castoldi, A.Galimberti, C.Guazzoni, P.Rehak, L.Strüder, R.Menk, "Energy-resolved X-ray radiography with Controlled-Drift Detectors at Sincrotrone Trieste", Nucl. Instr. And Meth. A510, 2003, 57-62.

[16] A. Castoldi, A. Galimberti, C. Guazzoni, P.Rehak, R. Hartmann, L.Strüder, "Multi-Linear Silicon Drift Detectors for X-ray and compton

imaging", Nucl. Instr. and Meth., Vol. 568, No. 1, 2006, pp. 89-95, Elsevier, Amsterdam, Olanda.
[17] C.von Zanthier, et al., "A fully depleted pn-junction CCD for Infrared-, UV- and X-ray detection", *Experimental astronomy*, 8:89-96, 1998.
[18] http://physics.nist.gov/PhysRefData/Xcom/Text/ XCOM.html
[19] D. E. Peplow and K. Verghese, "Measured molecular coherent scattering form factors of animal tissues, plastics and human breast tissue", Physics in Medicine and Biology, vol. 43, 1998, pp. 2431-2452.
[20] MATLAB, The language of technical computing, The Mathworks, Inc.
[21] C. H. Malden, R. D. Speller et al., "A CdZnTe array for the detection of explosive in baggage by energy dispersive X-ray diffraction signatures at multiple scatter angles", *Nucl. Instrum Meth*. A449, pp. 408-415, 2000.

TABLE I
COMPARISON OF THE DETAIL-TO-BACKGROUND CONTRAST OF THE MEAT SAMPLES SHOWN IN FIG. 7 AND FIG. 8

Meat Sample	Energy	Transmission image	Diffraction image	Contrast improvement[1]
First	18 keV	0.29±0.02	0.48±0.03	65%
First	26 keV	0.12±0.01	0.30±0.03	150%
Second	18 keV	0.33±0.03	0.46±0.05	39%
Second	26 keV	0.11± 0.01	0.29±0.02	163%

[1] Contrast improvement has been calculated as the difference between the contrast in diffraction images and the one in transmission images, normalized to the contrast in transmission images.

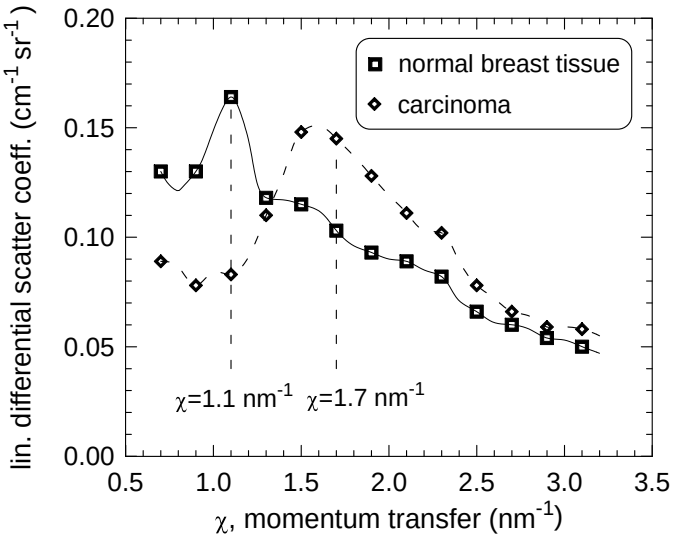

Fig. 1. Linear differential scatter coefficient of carcinoma and of normal breast tissue as a function of the momentum transfer. The location of the peaks at two different momentum transfers is shown [6].

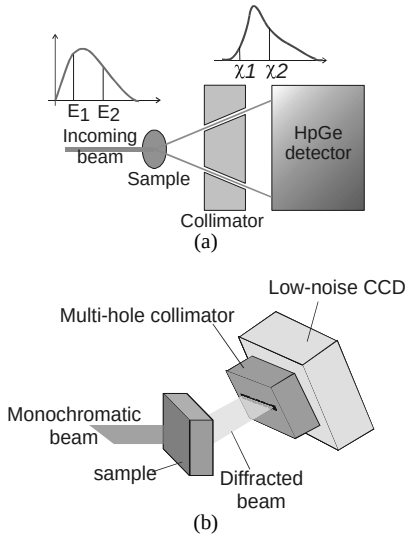

Fig. 2. Schematic diagram of the set-up used in a) Energy Dispersive DEBI, and b) Synchrotron Radiation DEBI.

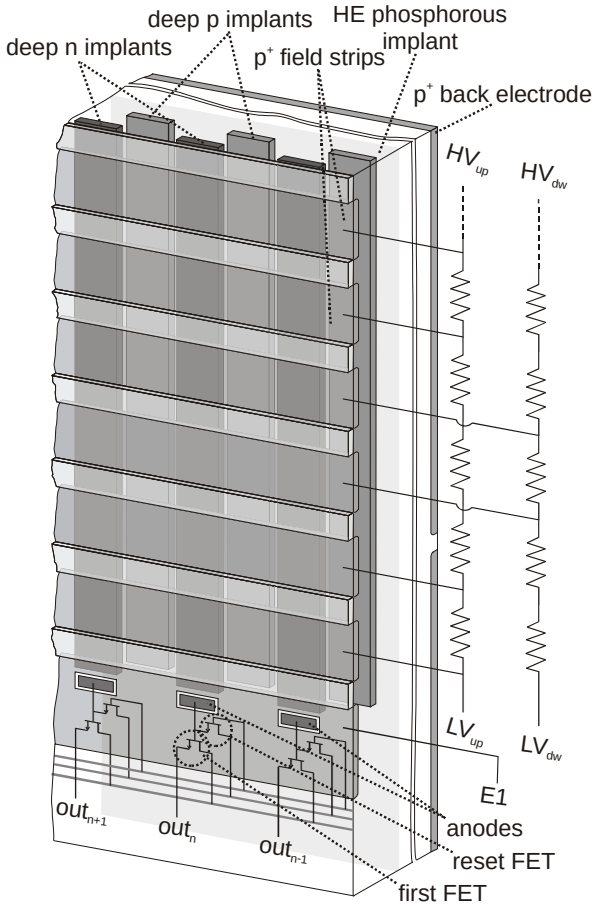

Fig. 3. Sketch of the Controlled-Drift Detector structure. Three drifting columns are shown with their readout section (collecting anode and integrated JFETs).

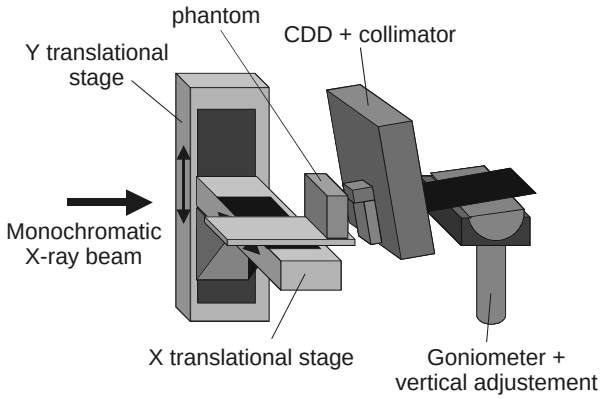

Fig. 4. Schematic drawing of the setup mounted at the SYRMEP beamline to evaluate the performances of the CDD in DEBI measurements.

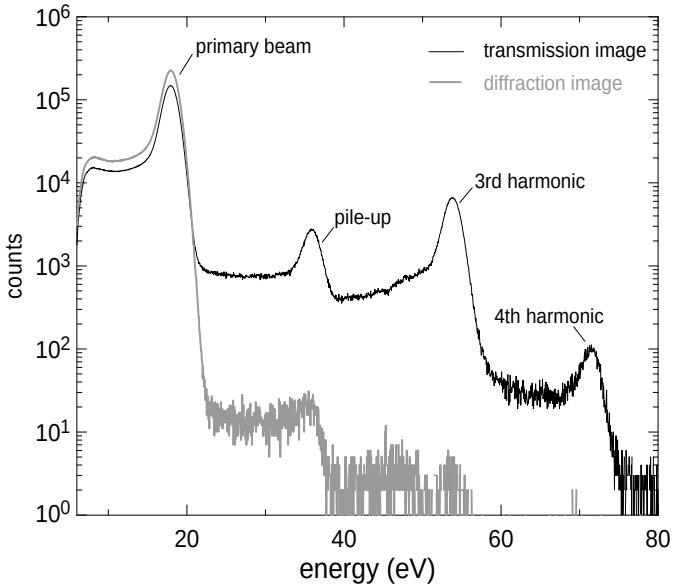

Fig. 5. Measured spectrum with the detector set both for transmission images acquisition (black line) and for diffraction images acquisition (gray line). The energy was set to 18 keV. The peak at twice the primary energy due to pulse pile-up in the detector is clearly visible in the energy spectrum related to both the transmission and the diffraction image. The peaks at three times and four times the primary beam energy are due to the higher harmonics transmitted by the monochromator (Si(111)).

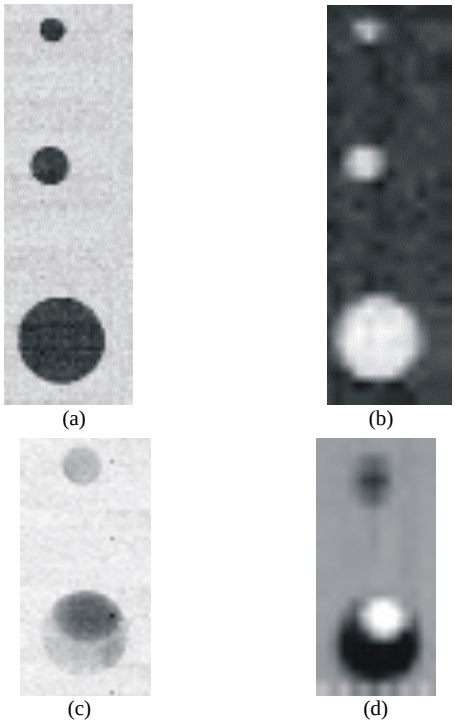

Fig. 6. Transmission and diffraction images of the perspex phantom at 18 keV. a) Transmission image – empty holes. b) Diffraction image – empty holes. c) Transmission image – holes filled with water. d) Diffraction image – holes filled with water. In c) and d) an air bubble is visible in the upper part of the larger hole

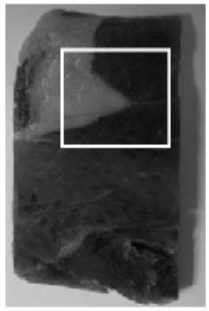

(a)

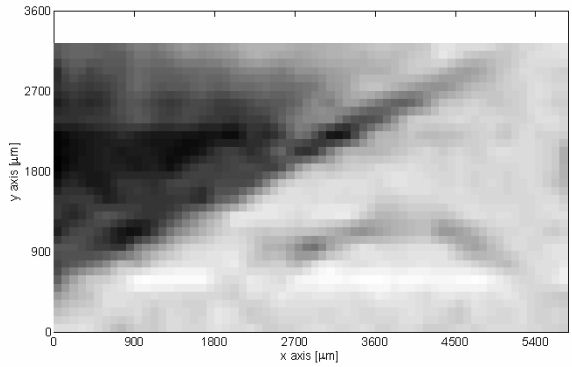

(b)

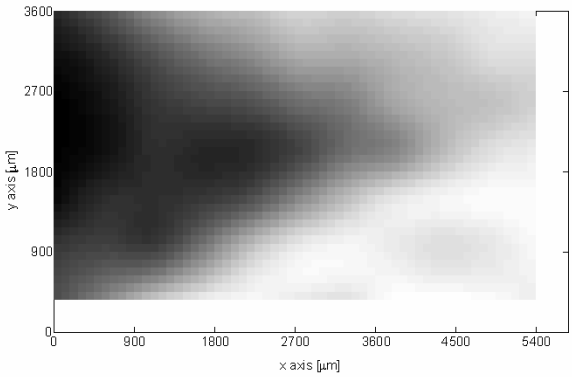

(c)

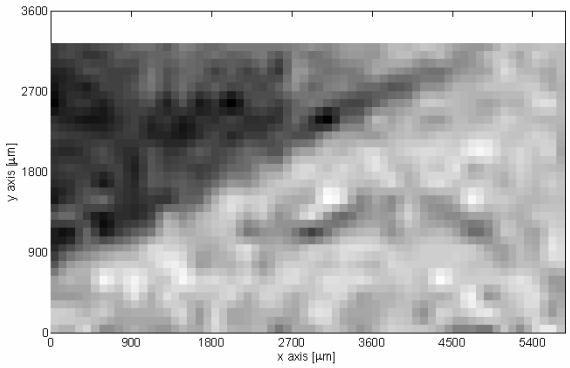

(d)

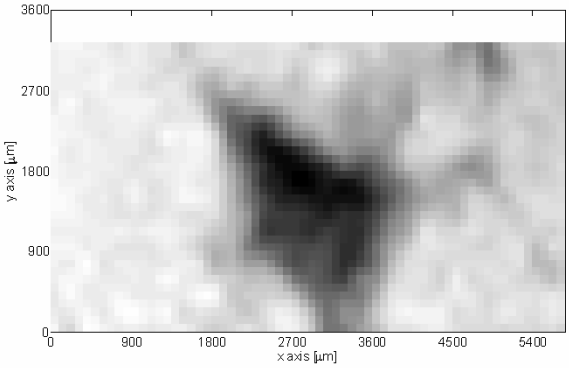

(b)

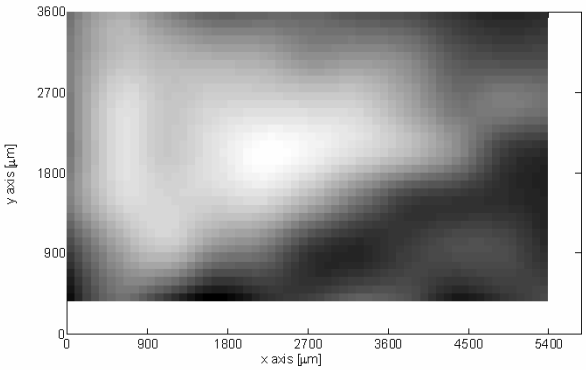

(e)

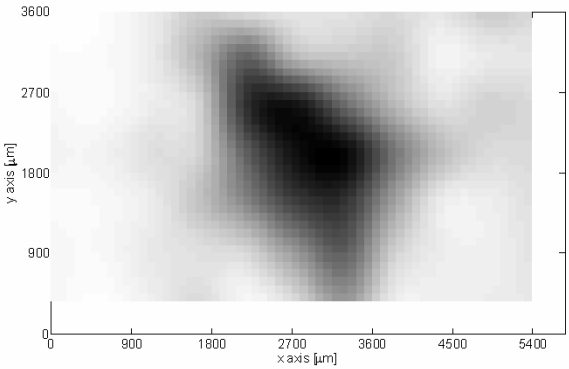

(c)

Fig. 7. a) Photograph of the first analysed meat sample, with the imaged detail marked. b) Transmission image at 18 keV. c) Diffraction image at 18 keV. d) Transmission image at 26 keV. e) Diffraction image at 26 keV. In all the images we have applied the MATLAB [20] bicubic interpolation algorithm.

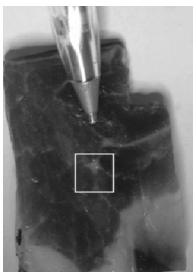

(a)

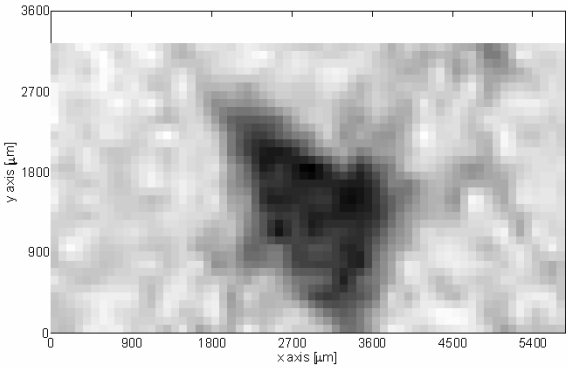

(d)

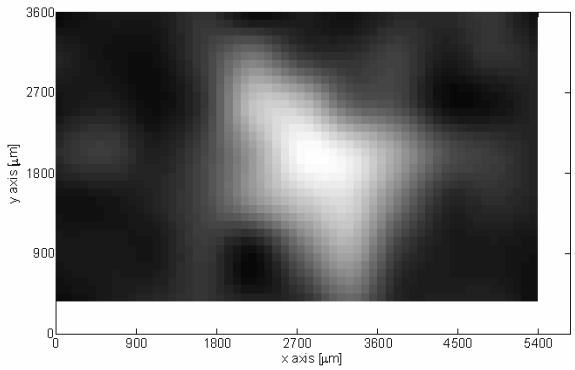

(e)

Fig. 8. a) Photograph of the second analysed meat sample, with the imaged detail marked. b) Transmission image at 18 keV. c) Diffraction image at 18 keV. d) Transmission image at 26 keV. e) Diffraction image at 26 keV. In all the images we have applied the MATLAB [20] bicubic interpolation algorithm.